

Effect of electron correlations on the electronic structure and phase stability of FeSe upon lattice expansion

S. L. Skornyakov,^{1,2} V. I. Anisimov,^{1,2} D. Vollhardt,³ and I. Leonov^{3,4}

¹*Institute of Metal Physics, Sofia Kovalevskaya Street 18, 620219 Yekaterinburg GSP-170, Russia*

²*Ural Federal University, 620002 Yekaterinburg, Russia*

³*Theoretical Physics III, Center for Electronic Correlations and Magnetism,
Institute of Physics, University of Augsburg, 86135 Augsburg, Germany*

⁴*Materials Modeling and Development Laboratory,
National University of Science and Technology 'MISIS', 119049 Moscow, Russia*

(Dated: March 10, 2017)

We present results of a detailed theoretical study of the electronic, magnetic, and structural properties of the chalcogenide parent system FeSe using a fully charge self-consistent implementation of the density functional theory plus dynamical mean-field theory (DFT+DMFT) method. In particular, we predict a remarkable change of the electronic structure of FeSe which is accompanied by a complete reconstruction of the Fermi surface topology (Lifshitz transition) upon a moderate expansion of the lattice volume. The phase transition results in a change of the in-plane magnetic nesting wave vector from (π, π) to $(\pi, 0)$ and is associated with a transition from itinerant to orbital-selective localized magnetic moments. We attribute this behavior to a correlation-induced shift of the van Hove singularity of the Fe t_2 bands at the M-point across the Fermi level. Our results reveal a strong orbital-selective renormalization of the effective mass m^*/m of the Fe 3d electrons upon expansion. The largest effect occurs in the Fe xy orbital, which gives rise to a non-Fermi-liquid-like behavior above the transition. The behavior of the momentum-resolved magnetic susceptibility $\chi(\mathbf{q})$ demonstrates that magnetic correlations are also characterized by a pronounced orbital selectivity, suggesting a spin-fluctuation origin of the nematic phase of paramagnetic FeSe. We conjecture that the anomalous behavior of FeSe upon expansion is associated with the proximity of the Fe t_2 van Hove singularity to the Fermi level and the sensitive dependence of its position on external conditions.

PACS numbers: 71.27.+a, 71.10.-w, 79.60.-i

I. INTRODUCTION

During the last decade the electronic, magnetic, and structural properties of the iron-based high-temperature superconducting pnictides and chalcogenides have been the subject of intensive research^{1,2}. These novel superconducting materials show certain similarities with the high- T_c cuprate superconductors. Indeed, the iron-based superconductors (FeSC) adopt a quasi 2D crystal structure where the iron atoms form a square lattice. The latter are separated by non-conducting layers containing, for example, alkali, alkaline earth, or rare earth elements, oxygen and/or fluorine. Moreover, the superconducting phase of these novel compounds often appears in the vicinity of a magnetic phase transition and/or structural instability. In particular, superconductivity in FeSCs often occurs as a result of the suppression of long-range, single-stripe antiferromagnetic (AF) order with a wave vector $Q_m = (\pi, \pi)$, due to electron/hole doping or pressure. This behavior has been regarded as evidence for the importance of spin fluctuations in the pairing of electrons in FeSCs.

The newly discovered Fe_{1+y}Se is structurally the simplest among the FeSCs³. At ambient pressure it has been found to become superconducting below $T_c \sim 8$ K close to its stoichiometric composition⁴. FeSe has the same layered structure as the pnictides, containing layers of edge-sharing FeSe_4 tetrahedra, but without separating

(non-conducting) layers³. Therefore FeSe is viewed as the parent compound of Fe-based superconductors which represents a minimal model material for understanding the mechanism of superconductivity of FeSCs. Moreover, FeSe itself exhibits remarkable physical properties. Its critical temperature $T_c \sim 8$ K at normal pressure increases to ~ 14 K upon isovalent substitution of Se with Te (corresponding to a negative chemical pressure, i.e., lattice expansion⁵), to ~ 37 K under compression⁶, to ~ 40 K by means of intercalation⁷, and all the way up to ~ 65 -109 K in the case of a monolayer⁸. In addition, FeSe has been found to exhibit a transition to a nematic phase below ~ 90 K in which the crystal (C_4) rotation symmetry is spontaneously broken⁹. Due to these intriguing properties FeSe has attracted much recent attention from both theory and experiment.

Angle-resolved photoemission spectroscopy (ARPES)¹⁰⁻¹² and band structure calculations¹³ reveal that the electronic structure of FeSe resembles that of the pnictides. It has a quasi 2D Fermi surface with three concentric hole pockets at the Brillouin zone Γ -point and two intersecting elliptical electron pockets centered at the M-point. The Fermi surface topology is characterized by an in-plane nesting wave vector (π, π) , consistent with s^\pm pairing symmetry¹⁴. Moreover, experimental studies of the spin excitation spectra of both pnictides and chalcogenides show an enhancement of short-range AFM spin fluctuations at vector (π, π)

near the T_c ¹⁵. These results suggest a common origin of superconductivity in pnictides and chalcogenides, for example due to spin fluctuations associated with the suppression of long-range magnetic order.

Unlike the majority of the FeSCs, FeSe is not magnetically ordered at ambient pressure and composition^{16,17}. Its isoelectronic counterpart FeTe, the end member of the Fe(Se,Te) series, is antiferromagnetic below the Néel temperature of 70 K. However, in contrast to the magnetic phases of the Fe-pnictides, FeTe exhibits double-stripe AF order with a $(\pi, 0)$ propagation vector¹⁸. Upon compression, FeTe exhibits a transition to a collapsed-tetragonal phase which is accompanied by a collapse of magnetic moments¹⁸. All this suggests a reconstruction of the electronic structure of Fe(Se,Te) upon change of the Se content or compression.

Photoemission and ARPES measurements of the electronic properties of Fe(Se,Te) reveal a significant narrowing of the Fe 3d bandwidth as compared to band structure calculations¹⁰. This corresponds to a strong orbital-dependent enhancement of the quasiparticle mass in the range ~ 3 -20 compared with the values obtained by electronic band structure techniques^{11,12}. Moreover, these experiments exhibit a damping of the coherent quasiparticles in Te-rich Fe(Se,Te), indicating a crossover from a coherent to incoherent behavior of the electronic structure. In addition, with increasing Te content, ARPES data for Fe(Se,Te) show a suppression of the spectral weight intensity associated with a Fermi surface pocket at the Brillouin zone M-point¹². This behavior is accompanied by an enhancement of spectral weight at the X-point, implying a possible doping-induced reconstruction of the electronic structure. Overall these experimental results point towards the importance of strong orbital-selective correlations.

State-of-the-art methods for the calculation of the electronic properties of strongly correlated systems, such as the density functional theory plus dynamical mean-field theory (DFT+DMFT) approach^{19,20} provide a good qualitative and even quantitative description of the band structure of FeSCs²¹. Applications of DFT+DMFT to FeSe yield a band mass enhancement in the range 2-5 and, in contrast to the pnictides, reveal the presence of a lower Hubbard band in the spectral function of FeSe^{22,23}. This clearly demonstrates the importance of correlation effects for the electronic properties of FeSe. Moreover, our recent DFT+DMFT calculations of the electronic properties and phase stability of FeSe predict that FeSe undergoes a phase transformation from a collapsed tetragonal to tetragonal phase upon expansion of the lattice²⁴. The transformation is found to be accompanied by a complete reconstruction of the topology of the Fermi surface (Lifshitz transition), a sharp increase of the local moments, and a change of magnetic correlations due to a transition of the in-plane magnetic wave vector from (π, π) to $(\pi, 0)$. This behavior was attributed to a correlation-induced shift of the van Hove singularity associated with the Fe xy and xz/yz orbitals at the

Brillouin zone M-point across the Fermi level²⁴.

The present study extends our previous investigation of FeSe²⁴. In particular, we now perform fully charge self-consistent DFT+DMFT calculations to determine the electronic properties and phase stability of paramagnetic FeSe. To this end, we take the crystal structure data for the paramagnetic tetragonal phase of FeSe from experiment³ and calculate the total energy as a function of volume. Our results reveal a substantial change of the total energy upon inclusion of the effects of charge redistribution caused by correlation effects. This proves the general importance of electronic correlations on the charge density and, hence, on the orbital occupancies. While this influence turns out to be negligible for the equilibrium volume, it becomes significant at higher volumes. At the same time the actual results for the electronic structure and phase stability show no qualitative difference compared to those calculated without charge self-consistency²⁴. Namely, the fully charge self-consistent calculations still find a structural phase transition upon expansion of the lattice, which is associated with a reconstruction of the topology of the Fermi surface (Lifshitz transition) and is accompanied by a sharp increase of the local moments. Indeed, our analysis of the Fermi surface topology and results for the spin susceptibility $\chi(\mathbf{q})$ support the previously suggested reconstruction of magnetic correlations from the in-plane magnetic wave vector (π, π) to $(\pi, 0)$, indicating a competition between these two magnetic instabilities²⁵. Moreover, we find that the individual orbitals contribute very differently to $\chi(\mathbf{q})$, a fact which may play a crucial role in explaining the observed nematicity in Fe(Se,Te) compounds⁹. Our calculations reveal a pronounced orbital-selective enhancement of electronic correlation upon expansion of the lattice. In particular, we observe a crossover from a Fermi-liquid with a weak self-energy-induced damping at the Fermi energy, to a non-Fermi-liquid like behavior where the self-energy almost diverges. The crossover is found to be associated with a transformation from an itinerant to localized magnetic moment behavior. Our results clearly demonstrate the crucial importance of orbital-selective correlations for a realistic description of the electronic and lattice properties of FeSe.

II. METHOD

In this paper, we employ a state-of-the-art DFT+DMFT computational scheme^{19,20}, which is fully self-consistent in the charge density, to determine the electronic properties and phase stability of paramagnetic tetragonal FeSe. It is implemented²⁶ within the non-spin polarized generalized gradient approximation (GGA) in DFT using plane-wave pseudopotentials²⁷. The approach combines a construction of the low-energy Hamiltonian for the partially filled Fe 3d and Se 4p orbitals in the basis of Wannier functions²⁸ with the

solution of the DMFT impurity problem using the continuous-time hybridization-expansion (segment) quantum Monte Carlo method²⁹. The effects caused by the correlation-induced charge redistribution are taken into account by solving the DFT+DMFT equations self-consistently in the charge density.

To investigate the structural stability, we use the atomic positions and the lattice parameter c/a of paramagnetic tetragonal FeSe taken from experiment³. To this end, we adopt the crystal structure data (space group $P4/nmm$, the lattice parameter ratio $c/a=1.458$, and the z -position of Se $z=0.266$) and calculate the total energy as a function of volume. In these calculations, we consider a uniform expansion or contraction of the lattice volume, i.e., only the lattice parameter a is varied, while the c/a ratio is fixed. We use the average Coulomb interaction $U = 3.5$ eV and Hund's exchange $J = 0.85$ eV for the Fe $3d$ shell, which are typical for the pnictides and chalcogenides according to different estimations²¹. The Coulomb interaction is treated in the density-density approximation. The spin-orbit coupling is neglected in these calculations. We employ the fully localized double-counting correction, evaluated from the self-consistently determined local occupancies, to account for the electronic interactions already described by DFT. The spectral functions and angle resolved spectra are evaluated from analytic continuation of the self-energy using Padé approximants.

We analyze possible magnetic instabilities of FeSe by calculating the static momentum-dependent susceptibility $\chi(\mathbf{q})$ within the particle-hole bubble approximation:

$$\chi(\mathbf{q}) = -k_B T \text{Tr} \sum_{\mathbf{q}, i\omega_n} \hat{G}(\mathbf{k}, i\omega_n) \hat{G}(\mathbf{k} + \mathbf{q}, i\omega_n). \quad (1)$$

Here T is the temperature, $\omega_n = (2n + 1)\pi k_B T$ is the Matsubara frequency, $\hat{G}(\mathbf{k}, i\omega_n)$ is the interacting lattice Green's function

$$\hat{G}(\mathbf{k}, i\omega_n) = [(i\omega_n + \mu)\hat{I} - \hat{H}(\mathbf{k}) - \hat{\Sigma}(i\omega_n)]^{-1}, \quad (2)$$

where μ is the chemical potential, $\hat{H}(\mathbf{k})$ is the effective low-energy Hamiltonian in Wannier basis, and $\hat{\Sigma}(i\omega_n)$ is the self-energy which includes an energy shift due to the double-counting correction term.

III. RESULTS

A. Phase stability and local magnetic moments

As a starting point, we compute the electronic structure and phase stability of paramagnetic FeSe. To this end, we evaluate the total energy of FeSe as a function of lattice volume by employing a fully charge self-consistent (csc) DFT+DMFT scheme^{30,31} and compare the result with that obtained from non-charge self-consistent (ncsc) DFT+DMFT calculations²⁴ (Fig. 1). The calculated

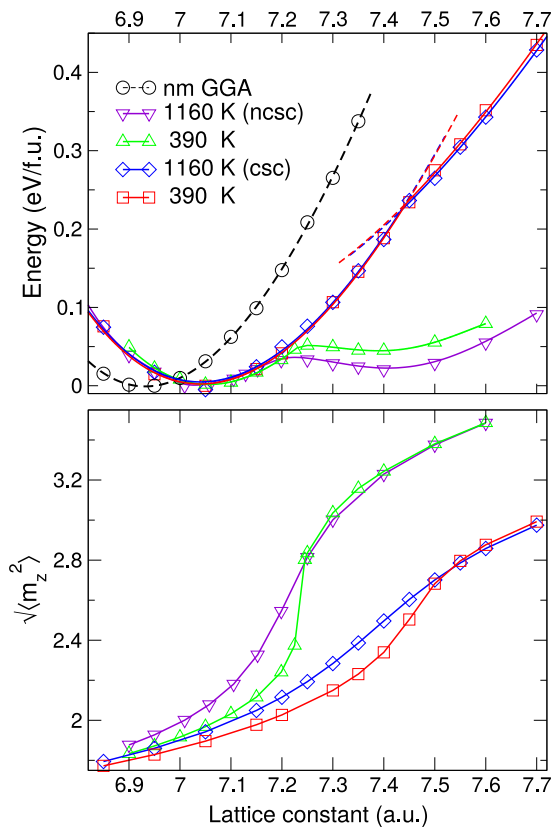


FIG. 1: (Color online) Total energy (upper panel) and instantaneous local magnetic moments $\sqrt{\langle m_z^2 \rangle}$ (lower panel) of paramagnetic FeSe as a function of lattice constant calculated by DFT+DMFT at a temperature $T = 390$ K with (csc) and without (ncsc) charge self-consistency. The total energy curve obtained with nonmagnetic GGA (nm GGA) is shown in the upper panel for comparison.

equilibrium lattice constant $a = 7.05$ a.u. at a temperature $T = 390$ K is in good quantitative agreement with the experimental data³, and to a good accuracy coincides with that obtained within ncsc DFT+DMFT²⁴. We note that within the nonmagnetic generalized gradient approximation (GGA) the equilibrium lattice constant is substantially underestimated²⁴. We also observe a substantial change of the total energy when the correlation-induced charge redistribution is taken into account. This clearly demonstrates the importance of the feedback of electronic correlations to the charge density. However, we find that this change is not very important for the actual value of the equilibrium volume. It only becomes notable at larger volumes, where it results in a shift of a lattice anomaly from 7.25 a.u. in the ncsc calculation to 7.45 in the csc calculations. We also estimate the bulk modulus K for the equilibrium phase by fitting the obtained energy-volume dependence using the third-order Birch-Murnaghan equation of state³². The computed value $K = 79$ GPa and its pressure derivative $K' \equiv dK/dP = 4.3$ at $T = 390$ K are close to those obtained by the ncsc calculations²⁴. The computed instan-

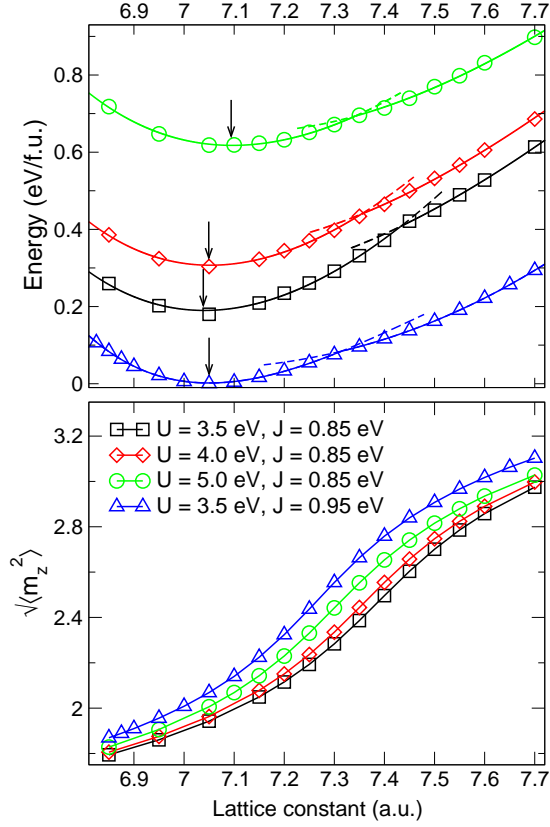


FIG. 2: (Color online) Total energy (upper panel) and instantaneous local magnetic moments $\sqrt{\langle m_z^2 \rangle}$ (lower panel) of paramagnetic FeSe calculated for different interaction parameters U and J at $T = 1160$ K using the charge self-consistent DFT+DMFT method. The arrows in the upper panel indicate the position of the energy minima.

taneous local magnetic moment $\sqrt{\langle m_z^2 \rangle}$ is about $1.9 \mu_B$, corresponding to a fluctuating local magnetic moment of $\sim 0.7 \mu_B$ ³³. Clearly, it is the inclusion of the local Coulomb interaction that provides an overall improved description of the properties of FeSe compared to the DFT results.

Both in the ncsc and csc DFT+DMFT calculations the local magnetic moment is found to increase upon expansion of the lattice volume (Fig. 1). We observe that charge self-consistency leads to a smoother evolution of the local moment and to a reduction of its absolute value in the whole range of lattice parameters. Moreover, ncsc and csc calculations both predict an iso-structural phase transition which is associated with a substantial increase of the local magnetic moment $\sqrt{\langle m_z^2 \rangle}$ upon expansion of the lattice. In view of the experimental findings for the volume and local magnetic moment of FeTe upon compression¹⁸, we interpret this behavior of FeSe as a transition from a collapsed-tetragonal (equilibrium volume) to tetragonal (expanded volume) phase which occurs upon expansion of the lattice. The expansion corresponds to a negative pressure of above ~ -7.6 GPa. The expanded-volume phase has a significantly smaller

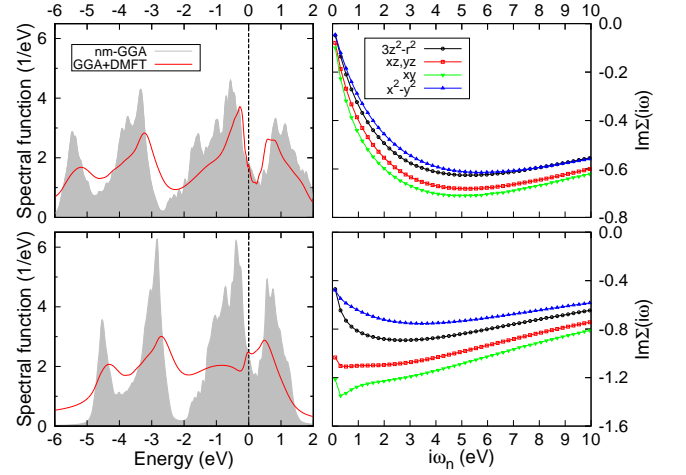


FIG. 3: (Color online) Left panels: Spectral functions of paramagnetic FeSe calculated within the charge self-consistent DFT+DMFT method (lines) in comparison with the DFT results (filled areas). Right panels: imaginary parts of the orbitals contributing to the self-energies on the Matsubara grid. Top row shows the results obtained for $a = 7.05$ a.u. Bottom row corresponds to $a = 7.6$ a.u.

bulk modulus of about 49 GPa. For $a = 7.6$ a.u. the calculated local magnetic moment is $\sim 2.9 \mu_B$ (the fluctuating local moment is $\sim 2.6 \mu_B$). Our results show that the transition is accompanied by an increase of the lattice constant from $a = 7.35$ a.u. to $a = 7.6$ a.u., corresponding to an increase of the lattice volume by 11 %. This transition persists even if the values of U and J are changed, as seen in Fig. 2. As expected, a stronger Coulomb repulsion U between the electrons leads to an increase of the equilibrium lattice volume. We also observe that for larger U values the phase transition occurs at lower volumes. In any case, the ncsc and csc calculations both predict a lattice and magnetic anomaly upon expansion of the unit cell volume. This anomaly is not found in spin polarized DFT calculations for the $(\pi, 0)$ and (π, π) antiferromagnetic configurations of iron moments³⁴, demonstrating the importance of electronic correlations in FeSe.

B. Spectral properties

To explore the mechanism behind this unusual volume dependence we calculate the spectral properties of FeSe and compare the results with those obtained from the ncsc DFT+DMFT calculations reported earlier²⁴. The spectral functions computed at the equilibrium volume ($a = 7.05$ a.u.) and above the transition ($a = 7.6$ a.u.) are shown in Fig. 3. Our results overall agree with those presented in Ref. 24. In particular, we find a substantial renormalization of the Fe 3d bands with respect to the DFT results. Indeed, such a behavior is common for the pnictides and chalcogenides and is in agreement with

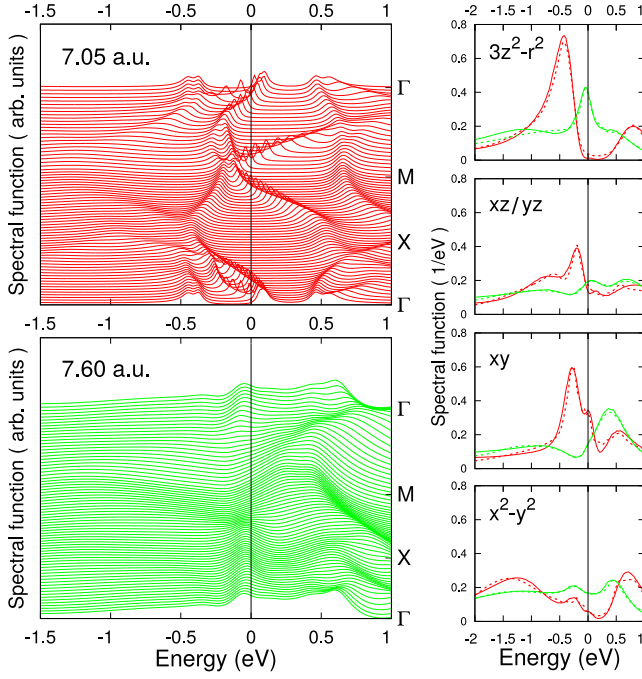


FIG. 4: (Color online) \mathbf{k} -resolved spectral functions (left column) and partial density of states (right column) of paramagnetic FeSe calculated by DFT+DMFT for $a = 7.05$ a.u. (red) and 7.6 a.u. (green). The orbitally-resolved contributions were evaluated using the maximum entropy method (solid line) and Padé approximants (broken line).

previous DFT+DMFT results for FeSe^{23,24}. Upon expansion of the lattice, we observe a strong redistribution of the spectral weight. In particular, it is seen that the sharp peak at -0.19 eV below the Fermi energy in the equilibrium volume phase is absent for larger volumes. This peak originates from the van Hove singularity of the Fe xz/yz and xy bands at the M-point. Moreover, for both phases the spectrum shows a broad feature at about -1.2 eV which is associated with the lower Hubbard band^{22,23}. The overall change of the spectral function shape upon expansion of the lattice agrees well with the evolution of photoemission spectra of Fe(Se,Te) series obtained upon increase of the Te content³⁵.

Next we calculate the \mathbf{k} -resolved spectral functions of paramagnetic FeSe along the high-symmetry directions of the Brillouin zone. In Fig. 4 (left panel) we present our results of the DFT+DMFT calculations for $a = 7.05$ a.u. and $a = 7.6$ a.u., respectively. The orbitally-resolved integrated spectral functions are shown in the right panel of Fig. 4. Our results for the electronic structure of FeSe are summarized in the left column of Fig. 5. Upon expansion of the lattice, we observe a remarkable reconstruction of the electronic structure of FeSe (see Figs. 4 and 5) which cannot be described by a simple rescaling or a shift of the non-correlated DFT band structure. We find that a substantial part of the spectral weight in the vicinity of E_F at the M-point is pushed from below to above the Fermi level, while the position of the energy bands near

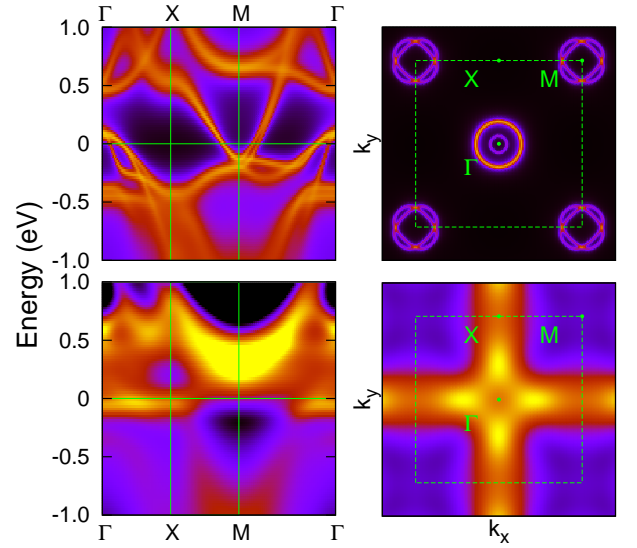


FIG. 5: (Color online) Electronic structure (left column) and Fermi surface (right column) of paramagnetic FeSe in the Γ -X-M plane of the reciprocal space as obtained using the charge self-consistent DFT+DMFT method at $T = 390$ K. Top row shows the results for $a = 7.05$ a.u. (low volume). Bottom row corresponds to $a = 7.6$ a.u. (high volume)

the Γ -point remains unaffected. This is associated with a correlation-induced shift of the van Hove singularity at the M-point above the Fermi level and implies an enhancement of the effect of electron correlations upon expansion of the lattice of FeSe. We also note that the correlation effects exhibit a pronounced orbital-dependent character.

To analyze this behavior in more detail we evaluate the Fermi surface of paramagnetic FeSe. In Fig. 5 (right column) we display the contour map of the spectral weight for the plane $k_z = 0$ obtained by integration of the spectral function $A(\mathbf{k}, \omega)$ over a small energy window (5 meV) around the Fermi level. Our results for the low-volume phase indicate a well-defined (coherent) Fermi surface (FS) which is similar to that in the pnictides³⁶. The FS exhibits two elliptic electron-like pockets at the M-point and two circular concentric hole pockets at the Γ -point. Similar to the results obtained from the ncsc calculations²⁴ the computed FS is characterized by a (π, π) nesting vector connecting the electron and hole sheets. A comparison of the calculated FS of paramagnetic FeSe with experiment shows that the size of the measured FS pocket is smaller than that obtained within DFT+DMFT. This is in accordance with previous DFT and DFT+DMFT studies^{22,37}, suggesting, e.g., the importance of non-local correlations effects, frustration magnetism³⁸, or spin-orbit interaction effects³⁹. Upon expansion of the lattice, we observe an abrupt change of the topology of the Fermi surface (Lifshitz transition). In particular, the spectral weight of the electron pockets centered at the M-point vanishes. The hole pocket encircling the Γ -point transforms into a large square-like FS

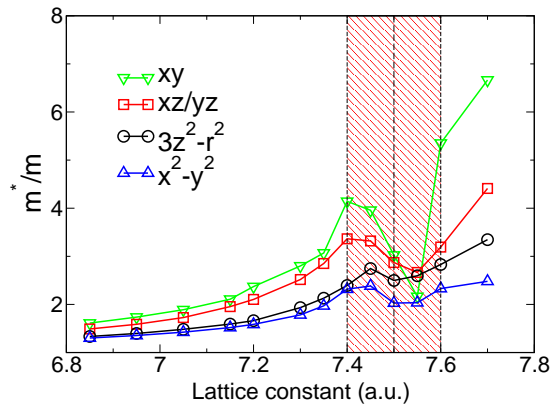


FIG. 6: (Color online) Orbitaly-resolved quasiparticle mass enhancement m^*/m of the Fe 3d states in paramagnetic FeSe as a function of lattice constant calculated by the charge self-consistent DFT+DMFT approach. The critical region associated with the electronic and structural transition is indicated by a red filled rectangle.

surrounding the M-point with the four pronounced spots around the Γ -point. This transition results in a change of the dominating nesting vector from (π, π) to $(\pi, 0)$. The observed topological change proceeds similar to the evolution of the experimental photoemission spectra^{11,12} of the doped $\text{FeSe}_{1-x}\text{Te}_x$ samples. These data confirm the emergence of the Fermi surface pocket at the X-point for large concentrations of Te for $x > 0.7$.

C. Orbital-selective renormalization

An expansion of the lattice also goes along with a remarkable orbital-selective renormalization of the Fe 3d bands (see Fig 6), indicating significantly stronger renormalization of the t_2 bands (xz/yz and xy) than of the e bands ($3z^2 - r^2$ and $x^2 - y^2$). In Fig. 3 (right column) we show the Fe 3d imaginary self-energies for the low- and high-volume phases, respectively. At the equilibrium volume, the self-energy obeys a Fermi-liquid-like behavior characterized by a weak damping of quasiparticles. By contrast, the expanded-volume phase shows a pronounced orbital-selective behavior, associated with a non-Fermi-liquid behavior of the t_2 orbitals. Indeed, the self-energies of the t_2 orbitals decrease with decreasing Matsubara frequency – and in the case of the self-energy of the xy -orbital even seems to diverge – but finally show an upturn at the lowest Matsubara frequency. At the same time, the e states remain Fermi-liquid-like, but with a damping which is about five times stronger than that in the equilibrium phase. These results agree well with an analysis of the band mass enhancement $m^*/m = 1 - \partial \text{Im}\Sigma(\omega)/\partial \omega|_{\omega=0}$, which provides a quantitative measure of the correlation strength. In Fig. 6 we display the computed mass enhancement m^*/m as a function of lattice constant. In the vicinity of the equilibrium lattice constant m^*/m lies in the range 1.5–2.

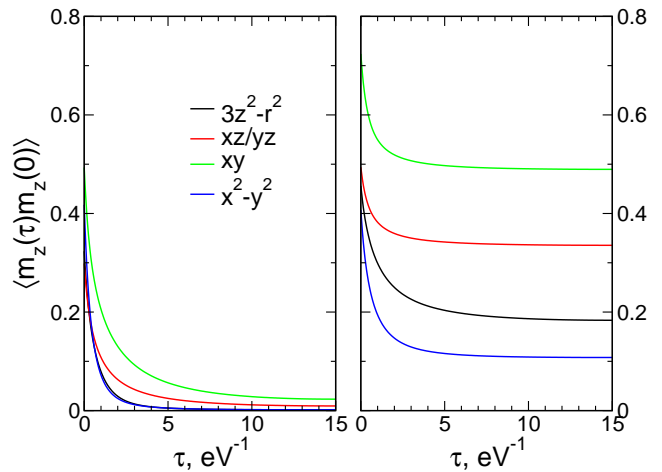


FIG. 7: (Color online) Orbitaly-resolved local spin correlation functions $\chi(\tau) = \langle \hat{m}_z(\tau) \hat{m}_z(0) \rangle$ of paramagnetic FeSe calculated using DFT+DMFT for the lattice constant $a = 7.05$ a.u. (left) and $a = 7.60$ a.u. (right).

Upon expansion of the lattice it shows a substantial increase followed by a critical region at $a \sim 7.5$ a.u. (where the electronic and structural transition occurs), which is characterized by a change of the sign of its derivative. Furthermore, the effective mass of the t_2 electrons exhibit larger renormalizations than in the e orbitals. Indeed, for the former it reaches ~ 6.5 and 4.5 for the Fe xy and xz/yz states, respectively.

D. Susceptibility

The electronic and structural phase transition is accompanied by a significant growth of the fluctuating local magnetic moment (see lower panel of Fig. 1). The transition is found to result in a crossover from an itinerant to localized moment behavior, as it is seen from the local spin susceptibility $\chi(\tau) = \langle \hat{m}_z(\tau) \hat{m}_z(0) \rangle$, where τ is the imaginary time. The results for the different orbital contributions are presented in Fig. 7. This behavior is consistent with the coherence-incoherence transition scenario which was found experimentally in the Fe(Se,Te) series¹². Moreover, our calculations reveal a strong orbital-selectivity in the formation of the local moments upon expansion of the lattice of FeSe. Here the xy orbital plays a predominant role, while the contribution of the xz/yz orbitals is substantially weaker. On the other hand, the e orbitals exhibit an itinerant moment behavior.

In addition, we compute the momentum-dependent local spin susceptibility $\chi(\mathbf{q})$ in the (q_x, q_y) plane for $q_z = 0$. Our results are presented in Fig. 8. The susceptibility calculated for the equilibrium volume shows a maximum at the corners of the tetragonal Brillouin zone at the M-points. This confirms that the leading magnetic instability of FeSe at ambient pressure occurs at the wave

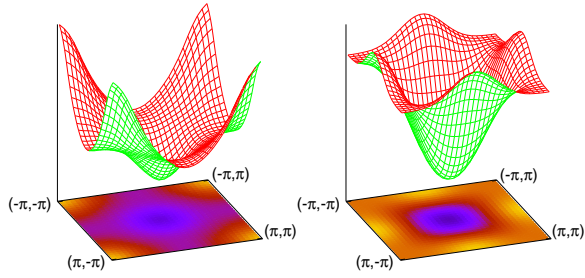


FIG. 8: (Color online) Momentum dependence of the local spin susceptibility $\chi(\mathbf{q})$ of paramagnetic FeSe calculated using the charge self-consistent DFT+DMFT method for $a = 7.05$ a.u. (left) and $a = 7.6$ a.u. (right).

vector (π, π) , in agreement with experiment¹⁵. An expansion of the lattice volume leads to a dramatic change of $\chi(\mathbf{q})$, associated with a suppression of the maximum at (π, π) and the development of a maximum at $(\pi, 0)$. This change of the magnetic correlations is associated with the change of the Fermi surface (Lifshitz transition) discussed above. The evolution of $\chi(\mathbf{q})$ qualitatively agrees with the experimentally observed transformation of magnetic correlations in the Fe(Se,Te) series¹⁷. Indeed, our results show a transition from (π, π) -type antiferromagnetic fluctuations in the paramagnetic tetragonal phase of FeSe to $(\pi, 0)$ -type magnetism upon expansion of the lattice.

Moreover, we calculate the orbital contributions of $\chi(\mathbf{q})$ along the Γ -X-M- Γ path (Fig. 9). For $a = 7.05$ a.u. we observe a strong orbital-selective behavior of magnetic correlations with a leading contribution originating from the Fe xy orbital. This orbital leads to a maximum of $\chi(\mathbf{q})$ at the M-point, confirming that magnetic correlations in FeSe are predominantly of the (π, π) -type. On the other hand, the behavior of $\chi(\mathbf{q})$ in the high volume phase is completely different. In particular, for $a = 7.6$ a.u. the leading contribution to $\chi(\mathbf{q})$ is due to the Fe $3z^2 - r^2$ orbital which varies only weakly along the Γ -X-M- Γ path. Our analysis shows that only the inclusion of all orbital contributions (especially of the $x^2 - y^2$ orbital contribution, which exhibits the most substantial variation in the reciprocal space and shows a maximum at the X-point) results in the $(\pi, 0)$ -type magnetic correlations prevalent in the high-volume phase of Fe(Se,Te).

Our results for $\chi(\mathbf{q})$ in Fig. 9 demonstrate that for $a = 7.05$ a.u. the xz and yz orbitals contribute very differently to $\chi(\mathbf{q})$ along the Γ -X-M direction. It will be interesting to check whether this finding, together with the symmetry-induced splitting between the xz/yz orbitals at the X point, can stabilize the observed nematicity in FeSe⁹, for example through the coupling of magnetic fluctuations to phonons near the X point.

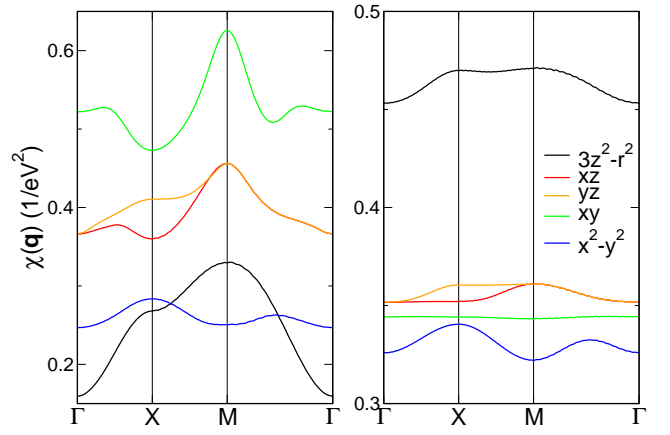


FIG. 9: (Color online) Orbitaly-resolved local spin susceptibility $\chi(\mathbf{q})$ of paramagnetic FeSe calculated along the Γ -X-M- Γ path using the charge self-consistent DFT+DMFT for $a = 7.05$ a.u. (left) and $a = 7.6$ a.u. (right).

IV. CONCLUSION

In conclusion, we studied the electronic structure and phase stability of the tetragonal paramagnetic phase of FeSe using a fully charge self-consistent implementation of the DFT+DMFT method. Our results demonstrate the importance of electron correlation effects which, in particular, trigger the anomalous behavior of FeSe upon expansion of the lattice volume. We note that such an expansion can be experimentally realized by the isovalent substitution of Se with Te. Our results also reveal a complete change of the electronic structure of paramagnetic FeSe upon a moderate expansion of the lattice (at ~ 7.6 GPa). This behavior is associated with a remarkable reconstruction of the Fermi surface topology (Lifshitz transition) of FeSe and is accompanied by a change of the in-plane magnetic nesting vector from (π, π) to $(\pi, 0)$, in agreement with experiment¹⁷. This behavior is intimately linked with an orbital-selective transition from itinerant to localized moment behavior, where the Fe xy orbitals contribute most strongly. The phase transformation is driven by a correlation-induced shift of the van Hove singularity of the Fe t_2 bands at the M-point across the Fermi level⁴⁰. We also observe a strong orbital-selective renormalization of the Fe $3d$ band structure, with the largest contribution coming again from the Fe xy orbital, which gives rise to a non-Fermi-liquid-like behavior above the transition.⁴¹ In view of our results the complex behavior of the chalcogenide parent system Fe(Se,Te), such as the anomalous increase of the superconducting temperature upon positive or negative pressure, appears to be associated with the proximity of the van Hove singularity of the Fe t_2 bands at the M-point to the Fermi level, and with the sensitivity of its position to external conditions⁴⁰. Furthermore, our results for the local spin susceptibility $\chi(\mathbf{q})$, which exhibits a strong splitting between the xz and yz orbitals near the

X-point, suggest a spin-fluctuation origin of the nematic phase of paramagnetic FeSe. This will be the subject of further investigations.

V. ACKNOWLEDGMENTS

We thank V. Tsurkan, J. Schmalian, and L. H. Tjeng for useful discussions. I.L. acknowledges support from

the Deutsche Forschungsgemeinschaft through Transregio TRR 80 and the Ministry of Education and Science of the Russian Federation in the framework of Increase Competitiveness Program of NUST "MISIS" (K3-2016-027), implemented by a governmental decree dated 16th of March 2013, N 211. D.V., S.L.S. and V.I.A. are grateful to the Deutsche Forschungsgemeinschaft for financial support through the Research Unit FOR 1346.

-
- ¹ Y. J. Kamihara, T. Watanabe, M. Hirano, and H. Hosono, *J. Am. Chem. Soc.* **130**, 3296 (2008); Z. A. Ren *et al.*, *Chin. Phys. Lett.* **25**, 2215 (2008); X. H. Chen, T. Wu, G. Wu, R. H. Liu, H. Chen, and D. F. Fang, *Nature (London)* **453**, 761 (2008).
 - ² J. Paglione and R. L. Greene, *Nat. Phys.* **6**, 645 (2010); D. N. Basov and A. V. Chubukov, *Nat. Phys.* **7**, 272 (2011); G. R. Stewart, *Rev. Mod. Phys.* **83**, 1589 (2011); P. Dai, J. Hu, and E. Dagotto, *Nat. Phys.* **8**, 709 (2012); Q. Si, R. Yu, and E. Abrahams, *Nat. Rev. Mater.* **1**, 16017 (2016).
 - ³ S. Margadonna *et al.*, *Chem. Commun. (Cambridge)* **43**, 5607 (2008); M. C. Lehman, A. Llobet, K. Horigane, and D. Louca, *J. Phys. Conf. Ser.* **251**, 012009 (2010).
 - ⁴ F. C. Hsu *et al.*, *Proc. Natl. Acad. Sci. U.S.A.* **105**, 14262 (2008).
 - ⁵ B. C. Sales, A. S. Sefat, M. A. McGuire, R. Y. Jin, D. Mandrus, and Y. Mozharivskyj, *Phys. Rev. B* **79**, 094521 (2009); A. Martinelli, A. Palenzona, M. Tropeano, C. Ferdeghini, M. Putti, M. R. Cimeterle, T. D. Nguyen, M. Af fronte, and C. Ritter, *Phys. Rev. B* **81**, 094115 (2010); V. Tsurkan, J. Deisenhofer, A. Günther, Ch. Kant, H.-A. Krug von Nidda, F. Schrettle, A. Loidl, *Eur. Phys. J. B* **79**, 289-299 (2011); U. R. Singh, S. C. White, S. Schmaus, V. Tsurkan, A. Loidl, J. Deisenhofer, and P. Wahl, *Phys. Rev. B* **88**, 155124 (2013).
 - ⁶ K. Miyoshi, K. Morishita, E. Mutou, M. Kondo, O. Seida, K. Fujiwara, J. Takeuchi, and S. Nishigori, *J. Phys. Soc. Jpn.* **83**, 013702 (2014).
 - ⁷ M. Burrard-Lucas, D. G. Free, S. J. Sedlmaier, J. D. Wright, S. J. Cassidy, Y. Hara, A. J. Corkett, T. Lancaster, P. J. Baker, S. J. Blundell, S. J. Clarke, *Nat. Mater.*, **12**, 15-19 (2013).
 - ⁸ S. Tan, Y. Zhang, M. Xia, Z. Ye, F. Chen, X. Xie, R. Peng, D. Xu, Q. Fan, H. Xu, J. Jiang, T. Zhang, X. Lai, T. Xiang, J. Hu, B. Xie, and D. Feng, *Nat. Mater.* **12**, 634-40 (2013).
 - ⁹ R. M. Fernandes, A. V. Chubukov, and J. Schmalian, *Nat. Phys.* **10**, 97 (2014); S.-H. Baek, D. V. Efremov, J. M. Ok, J. S. Kim, J. van den Brink, and B. Büchner, *Nat. Mater.* **14**, 210 (2015); A. E. Böhmer, T. Arai, F. Hardy, T. Hattori, T. Iye, T. Wolf, H. v. Löhneysen, K. Ishida, and C. Meingast, *Phys. Rev. Lett.* **114**, 027001 (2015); M. D. Watson, T. K. Kim, A. A. Haghighirad, N. R. Davies, A. McCollam, A. Narayanan, S. F. Blake, Y. L. Chen, S. Ghan-nadzadeh, A. J. Schofield, M. Hoesch, C. Meingast, T. Wolf, and A. I. Coldea, *Phys. Rev. B* **91**, 155106 (2015); Y. Yamakawa, S. Onari, and H. Kontani, *Phys. Rev. X* **6**, 021032 (2016).
 - ¹⁰ A. Tamai, A. Y. Ganin, E. Rozbicki, J. Bacsá, W. Meevasana, P. D. C. King, M. Caffio, R. Schaub, S. Margadonna, K. Prassides, M. J. Rosseinsky, and F. Baumberger, *Phys. Rev. Lett.* **104**, 097002 (2010); J. Malet, V. B. Zabolotnyy, D. V. Evtushinsky, S. Thirupathiah, A. U. B. Wolter, L. Harnagea, A. N. Yaresko, A. N. Vasiliev, D. A. Chareev, A. E. Bhmer, F. Hardy, T. Wolf, C. Meingast, E. D. L. Rienks, B. Büchner, and S. V. Borisenko, *Phys. Rev. B* **89**, 220506 (2014).
 - ¹¹ K. Nakayama *et al.*, *Phys. Rev. Lett.* **105**, 197001 (2010); F. Chen *et al.*, *Phys. Rev. B* **81**, 014526 (2010); Y. Zhang *et al.*, *Phys. Rev. B* **82**, 165113 (2010); J. Jiang, C. He, Y. Zhang, M. Xu, Q. Q. Ge, Z. R. Ye, F. Chen, B. P. Xie, and D. L. Feng, *Phys. Rev. B* **88**, 115130 (2013); K. Okazaki, *J. Phys. Conf. Ser.* **449**, 012019 (2013); E. Ieki *et al.*, *Phys. Rev. B* **89**, 140506(R) (2014); K. Nakayama, Y. Miyata, G. N. Phan, T. Sato, Y. Tanabe, T. Urata, K. Tanigaki, and T. Takahashi, *Phys. Rev. Lett.* **113**, 237001 (2014).
 - ¹² Z. K. Liu, R.-H. He, D. H. Lu, M. Yi, Y. L. Chen, M. Hashimoto, R. G. Moore, S.-K. Mo, E. A. Nowadnick, J. Hu, Z. Q. Mao, T. P. Devereaux, Z. Hussain, and Z.-X. Shen, *Phys. Rev. Lett.* **110**, 037003 (2013); Z. K. Liu, M. Yi, Y. Zhang, J. Hu, R. Yu, J.-X. Zhu, R.-H. He, Y. L. Chen, M. Hashimoto, R. G. Moore, S.-K. Mo, Z. Hussain, Q. Si, Z. Q. Mao, D. H. Lu, and Z.-X. Shen, *Phys. Rev. B* **92**, 235138 (2015).
 - ¹³ A. Subedi, L. Zhang, D. J. Singh, and M. H. Du, *Phys. Rev. B* **78**, 134514 (2008); K.-W. Lee, V. Pardo, and W. E. Pickett, *Phys. Rev. B* **78**, 174502 (2008); L. Zhang, D. J. Singh, and M. H. Du, *Phys. Rev. B* **79**, 012506 (2009).
 - ¹⁴ I. I. Mazin, D. J. Singh, M. D. Johannes, and M. H. Du, *Phys. Rev. Lett.* **101**, 057003 (2008); A. V. Chubukov, D. V. Efremov, and I. Eremin, *Phys. Rev. B* **78**, 134512 (2008).
 - ¹⁵ D. Christianson *et al.*, *Nature (London)* **456**, 930 (2008); M. D. Lumsden *et al.*, *Phys. Rev. Lett.* **102**, 107005 (2009); Y. M. Qiu *et al.*, *Phys. Rev. Lett.* **103**, 067008 (2009); M. D. Lumsden *et al.*, *Nat. Phys.* **6**, 182 (2010); M. C. Rahn, R. A. Ewings, S. J. Sedlmaier, S. J. Clarke, and A. T. Boothroyd, *Phys. Rev. B* **91**, 180501(R) (2015).
 - ¹⁶ S. Medvedev, T. M. McQueen, I. A. Troyan, T. Palasyuk, M. I. Erements, R. J. Cava, S. Naghavi, F. Casper, V. Ksenofontov, G. Wortmann, C. Felser, *Nat. Mater.* **8**, 630 (2009).
 - ¹⁷ W. Bao, Y. Qiu, Q. Huang, M. A. Green, P. Zajdel, M. R. Fitzsimmons, M. Zhernenkov, S. Chang, M. Fang, B. Qian, E. K. Vehstedt, J. Yang, H. M. Pham, L. Spinu, and Z. Q. Mao, *Phys. Rev. Lett.* **102**, 247001 (2009); T. J. Liu, J. Hu, B. Qian, D. Fobes, Z. Q. Mao, W. Bao, M. Reehuis, S. A. J. Kimber, K. Prokeš, S. Matas, D. N. Argyriou, A. Hiess, A. Rotaru, H. Pham, L. Spinu, Y. Qiu, V. Thampy, A. T. Savici, J. A. Rodriguez, C. Broholm, *Nat. Mater.*

- 9, 718 (2010); O. J. Lipscombe, G. F. Chen, C. Fang, T. G. Perring, D. L. Abernathy, A. D. Christianson, T. Egami, N. Wang, J. Hu, and P. Dai, Phys. Rev. Lett. **106**, 057004 (2011); M. Enayat, Z. Sun, U. R. Singh, R. Aluru, S. Schmaus *et al.*, Science **345**, 653 (2014).
- ¹⁸ S. Li, C. de la Cruz, Q. Huang, Y. Chen, J. W. Lynn, J. Hu, Y.-L. Huang, F.-C. Hsu, K.-W. Yeh, M.-K. Wu, and P. Dai Phys. Rev. B **79**, 054503 (2009); C. Zhang, W. Yi, L. Sun, X.-J. Chen, R. J. Hemley, H.-K. Mao, W. Lu, X. Dong, L. Bai, J. Liu, A. F. Moreira Dos Santos, J. J. Molaison, C. A. Tulk, G. Chen, N. Wang, and Z. Zhao, Phys. Rev. B **80**, 144519 (2009).
- ¹⁹ W. Metzner and D. Vollhardt, Phys. Rev. Lett. **62**, 324 (1989); G. Kotliar and D. Vollhardt, Phys. Today **57**, 53 (2004); A. Georges, G. Kotliar, W. Krauth, and M. J. Rozenberg, Rev. Mod. Phys. **68**, 13 (1996).
- ²⁰ V. I. Anisimov, A. I. Poteryaev, M. A. Korotin, A. O. Anokhin, and G. Kotliar, J. Phys. Condens. Matter **9**, 7359 (1997); G. Kotliar, S. Y. Savrasov, K. Haule, V. S. Oudovenko, O. Parcollet, and C. A. Marianetti, Rev. Mod. Phys. **78**, 865 (2006); J. Kunes, I. Leonov, M. Kollar, K. Byczuk, V. I. Anisimov, and D. Vollhardt, Eur. Phys. J. Spec. Top. **180**, 5 (2009); I. Leonov, Phys. Rev. B **92**, 085142 (2015); I. Leonov, V. I. Anisimov, and D. Vollhardt, Phys. Rev. B **91**, 195115 (2015); I. Leonov, L. Pourovskii, A. Georges, and I. A. Abrikosov, Phys. Rev. B **94**, 155135 (2016).
- ²¹ K. Haule, J. H. Shim, and G. Kotliar, Phys. Rev. Lett. **100**, 226402 (2008); V. I. Anisimov, D. M. Korotin, M. A. Korotin, A. V. Kozhevnikov, J. Kuneš, A. O. Shorikov, S. L. Skornyakov, and S. V. Streltsov, J. Phys. Condens. Matter **21**, 075602 (2009); M. Aichhorn, L. Pourovskii, V. Vildosola, M. Ferrero, O. Parcollet, T. Miyake, A. Georges, and S. Biermann, Phys. Rev. B **80**, 085101 (2009); S. L. Skornyakov, A. V. Efremov, N. A. Skorikov, M. A. Korotin, Yu. A. Izyumov, V. I. Anisimov, A. V. Kozhevnikov, and D. Vollhardt, Phys. Rev. B **80**, 092501 (2009); S. L. Skornyakov, A. A. Katanin, and V. I. Anisimov, Phys. Rev. Lett. **106**, 047007 (2011); Z. P. Yin, K. Haule, and G. Kotliar, Nat. Mater. **10**, 932 (2011); Z. P. Yin, K. Haule, and G. Kotliar, Nat. Phys. **7**, 294 (2011); M. Aichhorn, L. Pourovskii, and A. Georges, Phys. Rev. B **84**, 054529 (2011); J. M. Tomczak, M. van Schilfhaarde, and G. Kotliar, Phys. Rev. Lett. **109**, 237010 (2012); Z. P. Yin, K. Haule, and G. Kotliar, Phys. Rev. B **86**, 195141 (2012); A. Georges, L. de Medici, and J. Mravlje, Annu. Rev. Condens. Matter Phys. **4**, 137 (2013); C. Zhang *et al.*, Phys. Rev. Lett. **112**, 217202 (2014); S. Mandal, R. E. Cohen, and K. Haule, Phys. Rev. B **89**, 220502(R) (2014); A. van Roekeghem, L. Vaugier, H. Jiang, and S. Biermann, Phys. Rev. B **94**, 125147 (2016).
- ²² M. D. Watson, S. Backes, A. A. Haghighirad, M. Hoesch, T. K. Kim, A. I. Coldea, and R. Valentí, Phys. Rev. B **95**, 081106(R) (2017).
- ²³ M. Aichhorn, S. Biermann, T. Miyake, A. Georges, and M. Imada, Phys. Rev. B **82**, 064504 (2010).
- ²⁴ I. Leonov, S.L. Skornyakov, V.I. Anisimov, D. Vollhardt, Phys. Rev. Lett. **115**, 106402 (2015).
- ²⁵ Q. Wang *et al.*, Nat. Comm. **7**, 12182 (2016).
- ²⁶ I. Leonov, N. Binggeli, Dm. Korotin, V. I. Anisimov, N. Stojić, and D. Vollhardt, Phys. Rev. Lett. **101**, 096405 (2008); I. Leonov, Dm. Korotin, N. Binggeli, V. I. Anisimov, and D. Vollhardt, Phys. Rev. B **81**, 075109 (2010).
- ²⁷ S. Baroni, S. de Gironcoli, A. Dal Corso, and P. Giannozzi, Rev. Mod. Phys. **73**, 515 (2001); P. Giannozzi *et al.*, J. Phys. Condens. Matter **21**, 395502 (2009).
- ²⁸ V. I. Anisimov, D. E. Kondakov, A. V. Kozhevnikov, I. A. Nekrasov, Z. V. Pchelkina, J. W. Allen, S.-K. Mo, H.-D. Kim, P. Metcalf, S. Suga, A. Sekiyama, G. Keller, I. Leonov, X. Ren, and D. Vollhardt, Phys. Rev. B **71**, 125119 (2005); Dm. Korotin, A. V. Kozhevnikov, S. L. Skornyakov, I. Leonov, N. Binggeli, V. I. Anisimov, and G. Trimarchi, Eur. Phys. J. B **65**, 91-98 (2008); G. Trimarchi, I. Leonov, N. Binggeli, Dm. Korotin, and V. I. Anisimov, J. Phys.: Condens. Matter **20**, 135227 (2008).
- ²⁹ P. Werner, A. Comanac, L. de Medici, M. Troyer, and A. J. Millis, Phys. Rev. Lett. **97**, 076405 (2006); E. Gull, A. J. Millis, A. I. Lichtenstein, A. N. Rubtsov, M. Troyer, and P. Werner, Rev. Mod. Phys. **83**, 349 (2011).
- ³⁰ I. Leonov, V. I. Anisimov, and D. Vollhardt Phys. Rev. B **91**, 195115 (2015).
- ³¹ J. Kuneš, I. Leonov, P. Augustinský, V. Krápek, M. Kollar, and D. Vollhardt (to be published).
- ³² F. Birch, Phys. Rev. **71**, 809 (1947).
- ³³ The fluctuating local magnetic moment is evaluated from the imaginary-time average of the local spin susceptibility $\chi(\tau) = \langle \hat{m}_z(\tau) \hat{m}_z(0) \rangle$ as $M_z = k_B T \int_0^{1/k_B T} \chi(\tau) d\tau$, where τ is the imaginary time.
- ³⁴ S. L. Skornyakov, I. Leonov, V. I. Anisimov, JETP Lett. **103**(4), 265 (2016).
- ³⁵ T. Yokoya, R. Yoshida, Y. Utsumi, K. Tsubota, H. Okazaki, T. Wakita, Y. Mizuguchi, Y. Takano, T. Muro, Y. Kato, Sci. Technol. Adv. Mater. **13**, 054403 (2012).
- ³⁶ I. I. Mazin, D. J. Singh, M. D. Johannes, and M. H. Du, Phys. Rev. Lett. **101**, 057003 (2008); A. V. Chubukov, D. V. Efremov, and I. Eremin, Phys. Rev. B **78**, 134512 (2008).
- ³⁷ M. D. Watson, T. K. Kim, L. C. Rhodes, M. Eschrig, M. Hoesch, A. A. Haghighirad, A. I. Coldea, Phys. Rev. B **94**, 201107 (2016).
- ³⁸ J. K. Glasbrenner, I. I. Mazin, H. O. Jeschke, P. J. Hirschfeld, R. M. Fernandes and R. Valentí, Nat. Phys. **11**, 953 (2015).
- ³⁹ S. V. Borisenko, D. V. Evtushinsky, Z.-H. Liu, I. Morozov, R. Kappenberger, S. Wurmehl, B. Büchner, A. N. Yaresko, T. K. Kim, M. Hoesch, T. Wolf, and N. D. Zhigadlo, Nat. Phys. **12**, 311 (2016).
- ⁴⁰ A. Charnukha, D. V. Evtushinsky, C. E. Matt, N. Xu, M. Shi, B. Büchner, N. D. Zhigadlo, B. Batlogg, and S. V. Borisenko, Sci. Rep. **5**, 18273 (2015).
- ⁴¹ Z. Wang, M. Schmidt, J. Fischer, V. Tsurkan, M. Greger, D. Vollhardt, A. Loidl, and J. Deisenhofer, Nat. Comm. **5**, 3202 (2014).